

# The effect of dynamical Bloch oscillations on optical-field-induced current in a wide-gap dielectric

Péter Földi,<sup>1,\*</sup> Mihály G. Benedict,<sup>1</sup> and Vladislav S. Yakovlev<sup>2,3,†</sup>

<sup>1</sup>*Department of Theoretical Physics, University of Szeged,  
Tisza Lajos körút 84-86, H-6720 Szeged, Hungary*

<sup>2</sup>*Ludwig-Maximilians-Universität, Am Coulombwall 1, 85748 Garching, Germany*

<sup>3</sup>*Max-Planck-Institut für Quantenoptik, Hans-Kopfermann-Straße 1, 85748 Garching, Germany*

We consider the motion of charge carriers in a bulk wide-gap dielectric interacting with a few-cycle laser pulse. A semiclassical model based on Bloch equations is applied to describe the emerging time dependent macroscopic currents for laser intensities close to the damage threshold. At such laser intensities, electrons can reach edges of the first Brillouin zone even for electron–phonon scattering rates as high as those known for SiO<sub>2</sub>. We find that, whenever this happens, Bragg-like reflections of electron waves, also known as Bloch oscillations, affect the dependence of the charge displaced by the laser pulse on its carrier–envelope phase.

## I. INTRODUCTION

The motion of conduction-band electrons in a crystalline solid is usually considered to be similar to that in free space, apart from scattering processes. The situation is radically different in the case where an external electric field is so strong that, in spite of scattering, an electron can acquire such a high crystal momentum that it reaches an edge of the first Brillouin zone. While the kinetic energy of a free electron exposed to a constant external field would indefinitely increase, an electron in a crystal first slows down until it reaches the top of the energy band, and then it moves in the opposite direction towards the bottom of the band. In the semiclassical picture neglecting scattering, the electron would move periodically back and forth between its initial and final positions. This phenomenon is known as Bloch oscillations<sup>1</sup>, and it leads to Wannier–Stark localization<sup>2</sup>. In the reduced band scheme, an electron reaching an edge of the first Brillouin zone continues its motion from the opposite side of the zone. In the real space, this corresponds to a Bragg-like reflection of an electron wave<sup>3</sup>. While Bloch oscillations and Wannier–Stark localization are usually considered in the case of a constant external field, essentially the same physical phenomena take place if the external field is time dependent. In this paper, we use the term ‘dynamical Bloch oscillations’ to describe phenomena that occur whenever an electron wave is reflected at an edge of the Brillouin zone.

Until recently, Bloch oscillations were thought to be impossible to observe in bulk solids because of scattering. The period of Bloch oscillations in a constant field  $F$  is given by  $T_B = h(eFa)^{-1}$ , where  $h$  is the Planck constant and  $a$  is a lattice period. To observe Bloch oscillations,  $T_B$  must be smaller than characteristic scattering and dephasing times, which are usually on the order of  $T_s \sim 10^{-13}$  s. This implies that the external field must be stronger than  $F \gtrsim h(eaT_s)^{-1} \sim 10^8$  V m<sup>-1</sup>. Such a strong constant field would destroy even wide-gap dielectrics. Therefore, over the last few decades, Bloch oscillations were predominantly studied in artificial peri-

odic structures, such as semiconductor superlattices<sup>4,5</sup>, a notable exception being the observation of partial Bloch oscillations in  $n$ -doped GaAs interacting with intense terahertz pulses<sup>6</sup>. A closely related phenomenon, optical Bloch oscillations, was observed in periodic waveguide structures<sup>7,8</sup>, periodic dielectric systems<sup>9</sup> and optical lattices fabricated from porous silicon<sup>10</sup>. Also, Bloch oscillations were also studied for ultracold atoms in optical superlattices<sup>11,12</sup>.

The situation has recently changed as intense few-cycle pulses were generated in the mid-infrared (MIR) spectral region<sup>13</sup>, and the duration of the shortest near-infrared (NIR) pulses approached one optical cycle<sup>14</sup>. Ghimire *et al.*<sup>15,16</sup> observed that anharmonicity in the motion of charge carriers created and driven by an intense MIR pulse in ZnO resulted in the generation of high-order harmonics<sup>17</sup> and a red-shift of absorption edge<sup>16</sup>. In their parameter regime, the field was intense enough to drive conduction electrons beyond the first Brillouin zone, so that Bloch oscillations were suggested to be responsible for the observed effects.

Very recently, Schiffrin *et al.*<sup>18</sup> found that a 4 fs NIR pulse with a peak electric field of 20 GV m<sup>-1</sup> can induce measurable currents in a SiO<sub>2</sub> sample. Furthermore, it has been found that these currents can be steered by controlling the carrier–envelope phase (CEP)<sup>19</sup> of laser pulses. These findings were interpreted in terms of Wannier–Stark states<sup>20</sup>.

While it remains debatable whether Bloch oscillations played a major role in these particular measurements, there is no doubt that intense few-cycle pulses enable experiments in the parameter regime where electrons in a bulk solid are accelerated beyond the first Brillouin zone. The purpose of this paper is to study some basic effects related to this parameter regime. In particular, we consider the role of electron scattering and dephasing.

Electron–phonon scattering rates are known to be particularly high for SiO<sub>2</sub> due to a strong coupling between conduction electrons and longitudinal optical (LO) phonons<sup>21,22</sup>. At the same time, we are not aware of any direct measurements of scattering rates for moderately

hot ( $E_{\text{kin}} \sim 1$  eV) electrons, which we consider in this paper, and there are still open questions related to the scattering of very hot conduction electrons<sup>23</sup>.

## II. THE SYSTEM AND THE MODEL

We consider the following model (see Fig. 1): the  $xy$  ( $z = 0$ ) plane is the surface of a dielectric. Short pulses with a stabilized CEP propagate along the  $z$ -axis and impinge on this surface. In our calculations, we assume that the external electric field within the sample is linearly polarized and given by  $\mathcal{E}_x(t) = \mathcal{E}_0 \cos(\omega_0 t + \varphi_{\text{CEP}}) \exp[-t^2/(2\tau^2)]$ ,  $\mathcal{E}_y = \mathcal{E}_z = 0$ .

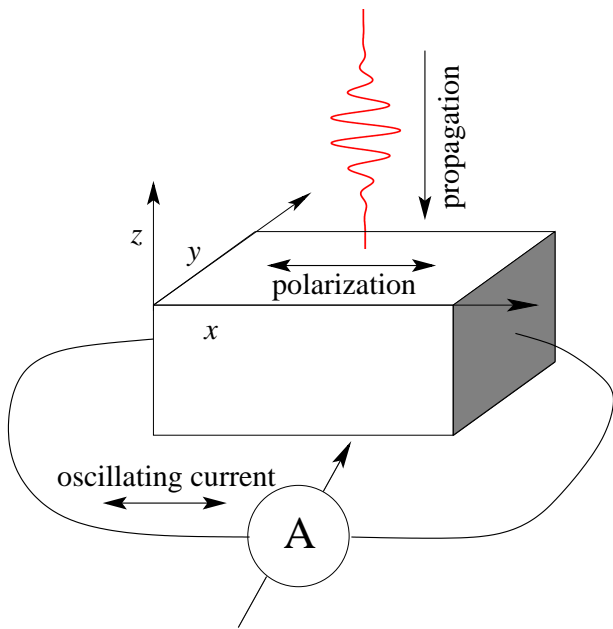


Figure 1. A schematic view of the creation and driving of macroscopic currents with a laser pulse. Measurements<sup>18</sup> yield the charge transferred by the pulse.

We adopt the two-band approximation and consider the electron motion in two spatial dimensions. At each moment  $t$ , we describe electronic excitations in the sample with the aid of quantum-mechanical density matrices

$$\rho(\mathbf{k}, t) = \begin{pmatrix} n_c(\mathbf{k}, t) & \mathcal{P}(\mathbf{k}, t) \\ \mathcal{P}^*(\mathbf{k}, t) & n_v(\mathbf{k}, t) \end{pmatrix}, \quad (1)$$

where  $n_c$ ,  $n_v$  correspond to the conduction and valence band populations, the off-diagonal element  $\mathcal{P}(\mathbf{k}, t)$  represents the interband coherence and the crystal momentum  $\mathbf{k}$  has two components:  $\mathbf{k} = (k_x, k_y)$ . The time dependence of the density matrix can be formally written as

$$\frac{\partial}{\partial t} \rho(\mathbf{k}, t) = \left( \frac{\partial \rho}{\partial t} \right)_{\text{exc}} + \left( \frac{\partial \rho}{\partial t} \right)_{\text{force}} + \left( \frac{\partial \rho}{\partial t} \right)_{\text{scatt}}. \quad (2)$$

The three terms on the right-hand side of this equation describe the effects that we take into account: photoexcitation, the acceleration of charge carriers by the external field and electron scattering, which acts as a 'friction force'. In the following, we use well established models to account for each of these phenomena; however, our model is rather phenomenological as we did not systematically derive it from first principles. The last two terms on the right-hand side of Eq. (2) are obtained from the standard single-band Boltzmann equation<sup>24</sup>. The role of the laser field is twofold here: besides driving charge carriers in the conduction and valence bands  $[(\partial_t \rho)_{\text{force}}]$ , it also drives interband transitions, i.e., populates the initially empty conduction band  $[(\partial_t \rho)_{\text{exc}}]$ .

It is common to describe strong-field excitations using rates for multiphoton or tunnelling transitions, but the applicability of this approach is very questionable for extremely short laser pulses at intensities where the Keldysh parameter is comparable to 1. Therefore, we use a quantum-mechanical model for the term  $(\partial_t \rho)_{\text{exc}}$  in Eq. (2), describing photoexcitation with  $\mathbf{k}$ -resolved optical Bloch equations<sup>25,26</sup> in the two-band approximation:

$$\begin{aligned} \left( \frac{\partial \mathcal{P}(\mathbf{k})}{\partial t} \right)_{\text{exc}} &= -\frac{i}{\hbar} [E_c(\mathbf{k}) - E_v(\mathbf{k}) - i\hbar\kappa] \mathcal{P}(\mathbf{k}) \\ &\quad - i[n_c(\mathbf{k}) - n_v(\mathbf{k})] d_{cv}(\mathbf{k}) \mathcal{E}(t), \\ \left( \frac{\partial n_c(\mathbf{k})}{\partial t} \right)_{\text{exc}} &= -2 \text{Im}[d_{cv}(\mathbf{k}) \mathcal{E}(t) \mathcal{P}^*(\mathbf{k})], \\ \left( \frac{\partial n_v(\mathbf{k})}{\partial t} \right)_{\text{exc}} &= -\frac{\partial n_c(\mathbf{k})}{\partial t}. \end{aligned} \quad (3)$$

Here,  $E_v(\mathbf{k})$  and  $E_c(\mathbf{k})$  are the energies of the valence and conduction bands, respectively,  $d_{cv}(\mathbf{k})$  is the  $x$ -component of the interband transition matrix element, and the phenomenological rate  $\kappa$  describes the decay of the interband coherences. We neglect interband relaxation (population decay) as it occurs on the picosecond to nanosecond time scale. For simplicity, we estimate the dependence of the dipole matrix elements on  $\mathbf{k}$  as  $d_{cv}(\mathbf{k}) = d_{cv}(0) \frac{E_c(0) - E_v(0)}{E_c(\mathbf{k}) - E_v(\mathbf{k})}$  (see Ref. 26). The actual value of  $d_{cv}(0)$  has a minor qualitative effect on our results, as long as saturation-related phenomena are negligible, i.e. the excited population is well below unity. In the following, we use  $d_{cv}(0) = 0.1$  atomic units. Note that Eqs. (3) make no use of the rotating wave approximation. This allows us to investigate dynamics that unfold within a single optical oscillation of the laser pulse (e.g. Ref. 27 contains a detailed discussion of related phenomena).

The external electric field not only causes transitions between the bands, but it also accelerates and decelerates charge carriers. These field-driven dynamics are accounted for by the second term in Eq. (2). We neglect off-diagonal terms in  $(\partial_t \rho)_{\text{force}}$  and evaluate the diagonal ones as

$$\left( \frac{\partial n_{v,c}(\mathbf{k})}{\partial t} \right)_{\text{force}} = -\frac{e}{\hbar} \mathcal{E}(t) \nabla_{\mathbf{k}} n_{v,c}(\mathbf{k}). \quad (4)$$

Note that  $\mathcal{E}(t)$  is the electric field *in the medium*, so that it is assumed to include both the screening field due to the collective electron response<sup>28</sup> and the field due to the polarization of the sample.

The third term in Eq. (2) accounts for the loss of in-

$$\left(\frac{\partial n_c(\mathbf{k})}{\partial t}\right)_{\text{scatt}} = \gamma_0 \sum_{\mathbf{q}} \delta(E(\mathbf{k} + \mathbf{q}) - E_c(\mathbf{k}) - \hbar\omega_{\text{LO}}) \frac{1}{q^2} \left\{ -N_{\mathbf{q}} n_c(\mathbf{k}) [1 - n_c(\mathbf{k} + \mathbf{q})] + (N_{\mathbf{q}} + 1) n_c(\mathbf{k} + \mathbf{q}) [1 - n_c(\mathbf{k})] \right\} + \gamma_0 \sum_{\mathbf{q}} \delta(E(\mathbf{k} - \mathbf{q}) - E_c(\mathbf{k}) + \hbar\omega_{\text{LO}}) \frac{1}{q^2} \left\{ -(N_{\mathbf{q}} + 1) n_c(\mathbf{k}) [1 - n_c(\mathbf{k} - \mathbf{q})] + N_{\mathbf{q}} n_c(\mathbf{k} - \mathbf{q}) [1 - n_c(\mathbf{k})] \right\}, \quad (5)$$

where  $\hbar\omega_{\text{LO}}$  denotes the energy of an LO phonon, which is assumed to be independent of the reciprocal-space vector  $\mathbf{q}$ . The related phonon density is denoted by  $N_{\mathbf{q}}$ , and  $\gamma_0$  is an electron–phonon coupling constant. For the sake of simplicity, we use a tight-binding-type dispersion relation, i.e. the energies  $E_{c,v}(\mathbf{k}) - E_{c,v}(0)$  are proportional to  $2 - \cos(k_x a) - \cos(k_y a)$ , where  $a$  is a lattice constant. At room temperature,  $N_{\mathbf{q}}$  is practically zero, so phonon emission processes (accompanied by electron scattering events with a loss of electron energy) dominate the scattering dynamics. Note that the scattering process described above qualitatively depends on the number of dimensions. By using a one-dimensional model, we would strongly underestimate momentum relaxation, as the probability of back-scattering ( $q \approx 2k$ ) is negligibly small for electrons with a kinetic energy larger than a fraction of electronvolt (eV). If there is more than one spatial dimension, electron deflection upon scattering results in a faster decrease of the net momentum. We chose to use two spatial dimensions in our calculations as a compromise between building a possibly realistic model for electron–phonon scattering and keeping computational time at an acceptable level.

The model described above allows us to calculate the rate of scattering on LO phonons  $\gamma(\mathbf{k})$ , which is proportional to  $\gamma_0$  appearing in Eq. (5). This scattering rate determines how fast the crystal momentum of an electron wave packet with a well-defined  $\mathbf{k}$  decreases as a consequence of scattering events. Our numerical calculations show, in accordance with the analytical results presented e.g. in Ref. 22, that the rate  $\gamma(\mathbf{k})$  has a pronounced minimum at  $\mathbf{k} = 0$ , being nearly constant ( $\gamma(\mathbf{k}) \approx \gamma$ ) for kinetic energies in the range between 0.5 eV and 2 eV. In the following, we use  $\gamma$  as a label to quantify the strength of electron–phonon interaction in different simulations, although we used  $\mathbf{k}$ -dependent scattering rates in our calculations. It must also be mentioned that the overall momentum of electrons distributed over a large part of the Brillouin zone may decrease at a rate that is much smaller than  $\gamma$  because, for a broad electron distribution, scattering events that increase the net momentum

traband coherence due to scattering, where longitudinal optical (LO) phonons are considered to play the major role. The electron–phonon interaction is described by the Fröhlich Hamiltonian, and standard methods<sup>26</sup> lead to the following dynamical equations:

are approximately as probable as those that decrease it.

For our simulations, we used material parameters that correspond to SiO<sub>2</sub>: a band gap of 9 eV, lattice period  $a = 0.5$  nm, two LO phonon modes with energies  $\hbar\omega_{\text{LO}} = 0.153$  and  $0.063$  eV, and a combined scattering rate equal to  $\gamma = 0.3$  fs<sup>-1</sup>. The laser pulse parameters correspond to the experiment described in Ref. 18:  $\omega_0 = 2.51$  fs<sup>-1</sup> and  $\tau = 2.3$  fs (FWHM = 3.8 fs). Note that in this case the band gap is more than five times larger than  $\hbar\omega_0$ ; thus, the excitation is far from being resonant or, in other words, it is a multiphoton process.

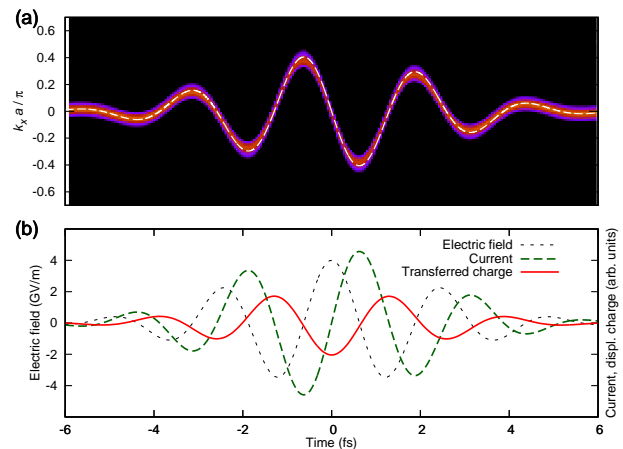


Figure 2. Laser-driven motion of conduction-band electrons that initially have a Gaussian distribution:  $n_c(\mathbf{k}, t_{\text{min}}) = \exp[-(k_x^2 + k_y^2)a^2\Delta^{-2}]$  with  $\Delta = 0.03$ . This simulation neglects photoexcitation and electron–phonon scattering. (a) The distribution of conduction electrons  $n_c(\mathbf{k}, t)$  in the  $k_y = 0$  plane. The dashed white line is the ‘semiclassical trajectory’ evaluated with the aid of the acceleration theorem (6). (b) The electric field  $\mathcal{E}_x(t)$  that drives the wave packet, the current density  $j_x(t)$  and the time dependent transferred charge  $Q(t)$ . The parameters are  $\mathcal{E}_0 = 4$  GV m<sup>-1</sup>,  $\varphi_{\text{CEP}} = 0$ ,  $\tau = 2.3$  fs.

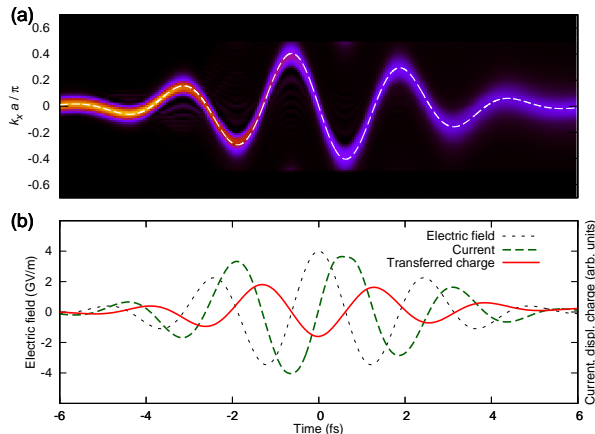


Figure 3. Time evolution of a wave packet initially centred at  $\mathbf{k} = 0$  in a simulation that neglects photoexcitation but takes electron-phonon scattering into account.  $\gamma = 0.3 \text{ fs}^{-1}$ ; all other parameters are the same as in Fig. 2. Electron scattering along both  $k_x$  and  $k_y$  is responsible for the gradual reduction of the reciprocal-space electron distribution  $n_c(\mathbf{k}, t)$  towards the end of the laser pulse, but it has a relatively weak effect on  $j_x(t)$ .

### III. RESULTS

#### A. Electron acceleration in the laser field

Before we present simulations where a laser pulse creates and drives charge carriers, let us consider the laser-driven motion of initially free electrons neglecting interband transitions. Similar simulations can be found in Ref. 29. As an example, we take the initial distribution of conduction electrons as a Gaussian wave packet centred at  $\mathbf{k} = 0$ , neglect the terms  $(\partial_t \rho)_{\text{exc}}$  and  $(\partial_t \rho)_{\text{scatt}}$  in Eq. (2) and model the time evolution of the electron wave packet by solving Eq. (4). We plot the distribution of conduction electrons in false-colour diagrams, where colours vary from black through red to yellow as the electron population  $n_c(\mathbf{k}, t)$  grows from zero to its maximal value. The top panel of Fig. 2 presents such a diagram in the plane  $k_y = 0$ . In this example, the distribution remains localized in the reciprocal space, and it is dynamically shifted by the field of the laser pulse. The reciprocal-space motion of the wave packet is appropriately described by the ‘acceleration theorem’<sup>24</sup>:

$$\frac{\partial \mathbf{k}}{\partial t} = -\frac{e}{\hbar} \mathcal{E}(t). \quad (6)$$

A solution of this equation with the initial condition  $k(t_{\text{min}}) = 0$  is shown by the dashed white line in Fig. 2. This solution can be regarded as a trajectory of a ‘classical particle’ in the reciprocal space. Let us note that as long as neither scattering nor excitation is taken into account, there is a simple scaling in the model: increasing both the carrier frequency  $\omega_0$  and the amplitude of the

laser pulse  $\mathcal{E}_0$  by a certain factor is equivalent to choosing a new unit of time in Eq. (2), and it does not change the maximal crystal momentum that a wave packet can reach in the reciprocal space.

Having evaluated the time evolution of the density matrix, we are able to investigate measurable physical quantities.

The number of electrons excited per unit cell is given by

$$\langle n_c \rangle = \Omega^{-1} \int n_c(\mathbf{k}) d^2 \mathbf{k} \quad (7)$$

with

$$\Omega = \int d^2 \mathbf{k}. \quad (8)$$

The electric current per unit cell  $\mathbf{j}(t)$  is a sum of contributions from conduction-band electrons

$$\mathbf{j}_c(t) = \Omega^{-1} \int_{\text{BZ}} e \mathbf{v}_c(\mathbf{k}) n_c(\mathbf{k}, t) d^2 \mathbf{k}, \quad (9)$$

valence-band holes

$$\mathbf{j}_v(t) = \Omega^{-1} \int_{\text{BZ}} e \mathbf{v}_v(\mathbf{k}) n_v(\mathbf{k}, t) d^2 \mathbf{k}, \quad (10)$$

and interband coherences

$$\mathbf{j}_{cv}(t) = 2\hbar^{-1} \Omega^{-1} \text{Im} \left\{ \int_{\text{BZ}} \mathcal{P}(\mathbf{k}, t) \mathbf{d}_{cv}(\mathbf{k}) \times [E_v(\mathbf{k}) - E_c(\mathbf{k})] d^2 \mathbf{k} \right\}, \quad (11)$$

where the integrals are taken over the first Brillouin zone (in the  $k_x$  and  $k_y$  directions, in accordance with our 2D model), and the velocity distributions are given by  $\mathbf{v}_{v,c}(\mathbf{k}) = \hbar^{-1} \nabla_{\mathbf{k}} E_{v,c}(\mathbf{k})$ . Equations (9)-(11) result from evaluating the expectation value of the current operator averaged over a unit cell for a state described by the density matrix (1). Integrating the current density with respect to time, we obtain the charge (per unit cell) that flows through a surface perpendicular to the  $x$ -axis:  $Q(t) = \int_{-\infty}^t j_x(t') dt' = Q_c(t) + Q_v(t) + Q_{cv}(t)$ , where  $j_x$  denotes the  $x$ -component of the total current density  $\mathbf{j} = \mathbf{j}_c + \mathbf{j}_v + \mathbf{j}_{cv}$ . It is the charge displaced by the laser pulse  $Q = Q(\infty)$  that can be measured in experiments<sup>18</sup>. In the following, we assume that  $\mathbf{j}_c$  gives the dominant contribution to  $Q$ . Indeed,  $\mathbf{j}_v$  is negligible in comparison with  $\mathbf{j}_c$  due to the low mobility of holes in the valence band, while  $\mathbf{j}_{cv}$  mainly describes the polarization response of valence-band electrons; according to our calculations,  $Q_{cv}(t)$  is proportional to the applied field within a relative error of no more than 5% up to a field amplitude of  $\mathcal{E}_0 = 25 \text{ GV m}^{-1}$ ,  $Q_{cv}(\infty)$  being negligibly small in comparison to  $Q_c(\infty)$ . Keeping this in mind, we restrict our analysis to  $\mathbf{j}_c$  and  $Q_c$ , referring to them as

'current density' and 'transferred charge', respectively. As long as the laser field is linearly polarized and the medium is isotropic,  $\mathbf{j}_c$  is parallel to the  $x$ -axis. The current density  $j_x(t)$  and the charge transferred along the laser polarization are shown in Fig. 2(b) together with the electric field of the laser pulse, which is depicted by the dashed black line.

In Fig. 3, we show the effects of electron–phonon scattering on the dynamics of a conduction-band wave packet initially centred at  $\mathbf{k} = 0$ . A comparison with Fig. 2, where scattering was neglected, reveals that the electron–phonon interaction disperses the electron wave packet, but it has a relatively weak effect on  $j_x(t)$ , decreasing the amplitude of its oscillations by merely 20%.

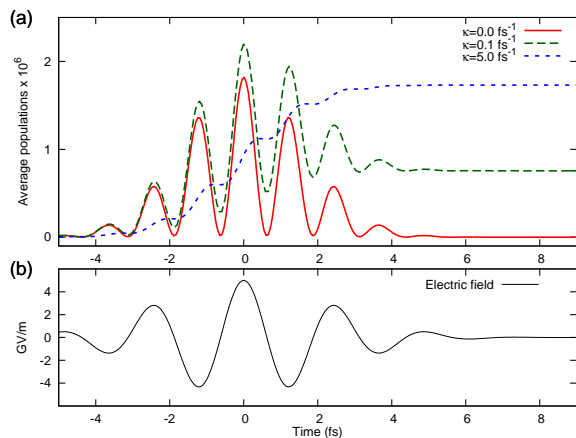


Figure 4. Average conduction-band population (7) for different interband coherence relaxation rates  $\kappa$ . For  $\kappa = 5.0 \text{ fs}^{-1}$  (dashed blue curve), we plot  $0.05\langle n_c \rangle$ . The parameters are  $\mathcal{E}_0 = 5 \text{ GV m}^{-1}$ ,  $\varphi_{\text{CEP}} = 0$ ,  $\tau = 2.3 \text{ fs}$ ,  $\gamma = 0.3 \text{ fs}^{-1}$ .

### B. Nonresonant interband excitations

In order to expose a medium to a very intense laser field without destroying it, the medium must be possibly transparent, so that little energy will remain in the medium after the interaction with the pulse. This implies that the laser frequency  $\omega_0$  should be much smaller than the band gap. This is why we are interested in studying nonresonant excitations. With our laser parameters, it takes more than five laser photons to bridge the band gap of  $\text{SiO}_2$ .

The dynamics of interband excitations predicted by our model are shown in Fig. 4. For  $\kappa = 0$ , Eq. (3) describes a completely coherent excitation process, with the average population in the conduction band being roughly proportional to the laser intensity. These periodic excitations and deexcitations are sometimes referred to as 'virtual excitations', as they largely represent distortions of initial electronic states. Both virtual and real excitations contribute to photocurrents<sup>30</sup>. In the opposite

extreme, if we assume an unrealistically fast decoherence  $\kappa = 5 \text{ fs}^{-1}$ , the conduction band population becomes a monotonically increasing step-like function of time. Little is known about ultrafast dephasing in  $\text{SiO}_2$ , so we use  $\kappa = 0.1 \text{ fs}^{-1}$  for our further simulations as a value that corresponds to an intermediate regime of interband excitations.

### C. Laser-driven motion of photoexcited charge carriers and the effect of the carrier–envelope phase

Here, we investigate the outcomes of our model with all three terms of Eq. (2) being taken into account. The most interesting result of combining excitation and laser-driven motion is that this may result in a nonzero charge  $Q$  transferred by a laser pulse—a transport effect that does not occur in simulations neglecting interband transitions, as Figs. 2 and 3 illustrate. In this section, we show that this is a combination of interband transitions and a dispersion law that determines the transferred charge.

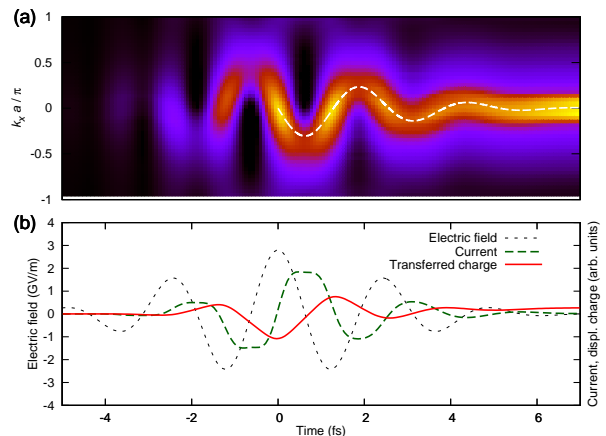


Figure 5. (a) Time evolution of the conduction-band electron population that emerges due to multiphoton excitations. The cross section in the  $k_x$  direction (parallel to the polarization of the laser field) is shown for the following parameters:  $\mathcal{E}_0 = 3 \text{ GV m}^{-1}$ ,  $\varphi_{\text{CEP}} = 0$ ,  $\tau = 2.3 \text{ fs}$ ,  $\kappa = 0.1 \text{ fs}^{-1}$ ,  $\gamma = 0.3 \text{ fs}^{-1}$ . The dashed white line represents a semiclassical trajectory released at  $t = 0$  with  $\mathbf{k} = 0$ . (b) The electric field of the laser pulse  $\mathcal{E}_x(t)$ , the induced current density  $j_x(t)$  and the transferred charge  $Q(t)$  as functions of time.

In the upper panels of Figs. 5 and 6, we show  $n_c(k_x, t)$  obtained in simulations that account for all the relevant processes: multiphoton excitations, light-driven motion of charge carriers, dephasing and electron–phonon scattering. The simulation were performed for a 'cosine' ( $\varphi_{\text{CEP}} = 0$ ) and a 'sine' ( $\varphi_{\text{CEP}} = \pi/2$ ) laser pulses, respectively. The lower panels of the figures show the electric field of the laser pulse  $\mathcal{E}_x(t)$ , the induced current density  $j_x(t)$  and the transferred charge  $Q(t)$  as functions of time. Because of scattering, the current density at the

end of each simulation quickly approaches zero, but the final value of the transferred charge is in general nonzero, and it has a significantly higher value for the cosine pulse (Fig. 5).

The dashed lines in Figs. 5(a) and 6(a) represent 'semiclassical electron trajectories' released at a peak of the electric field, which are solutions of Eq. (6) with the initial condition  $\mathbf{k}(t_0) = 0$ , the initial time being  $t_0 = 0$  for the cosine pulse and  $t_0 = -\pi(2\omega_0)^{-1}$  for the sine pulse. Even without taking scattering into account, this semiclassical analysis can be used to explain many features observed in our calculations. In this picture, the contribution from a particular electron to the transferred charge at a final time  $t_{\max}$  is determined by the semiclassical electron displacement:

$$\mathbf{s}(t_0) = \int_{t_0}^{t_{\max}} \mathbf{v}_c(\mathbf{k}(t)) dt, \quad (12)$$

where  $t_0$  is a time when the electron appeared in the conduction band,  $\mathbf{k}(t)$  satisfies Eq. (6),  $\mathbf{v}_c(\mathbf{k}) = \hbar^{-1}\nabla_{\mathbf{k}}E_c(\mathbf{k})$  and an implicit assumption was made that the initial velocity of the electron is zero. In the case of a short cosine pulse, the central half-cycle of the electric field has a significantly higher amplitude than any other half-cycle. Consequently, there is one dominant semiclassical trajectory that starts at the peak of the main half-cycle. A simple calculation shows that, in our example, the semiclassical displacement associated with this trajectory is negative, which agrees with the positive final transferred charge in Fig. 5. For a short sine pulse, there are two dominant trajectories which start at the peaks of the two most pronounced half-cycles of the electric field. The electron displacements associated with these trajectories have opposite signs and add 'destructively' in the case shown in Fig. 6. This explains why the magnitude of the net transferred charge is considerably smaller for  $\varphi_{\text{CEP}} = \pi/2$  than for  $\varphi_{\text{CEP}} = 0$ .

We further elaborate on the role of the CEP in Fig. 7, where we plot  $Q(\varphi_{\text{CEP}})$  for different values of  $\kappa$  and  $\gamma$ . From this figure, one can see that  $Q(\varphi_{\text{CEP}} + \pi) = -Q(\varphi_{\text{CEP}})$ , which is a direct consequence of symmetry: adding  $\pi$  to the CEP is equivalent to substituting  $\mathcal{E}(t)$  with  $-\mathcal{E}(t)$ , which is equivalent to replacing  $x$  with  $-x$  in our symmetric arrangement. One also infers from Fig. 7 that the relaxation rate of interband coherences influences the positions of minima and maxima of  $Q(\varphi_{\text{CEP}})$ , which is not the case for the phonon scattering rate  $\gamma$ .

Increasing the amplitude of the input laser fields, we reach the regime where even electrons initially excited in the middle of the Brillouin zone experience reflections at its edges during the laser pulse—dynamical Bloch oscillations (DBOs) take place. This is illustrated in Fig. 8, where we plot the outcomes of a simulation with a laser pulse that has a peak amplitude of the electric field of  $10 \text{ GV m}^{-1}$ , the other parameters being the same as in the previous simulations. DBOs occur in spite of the fact that we use a fairly large value for the electron-phonon scattering rate ( $\gamma = 0.3 \text{ fs}^{-1}$ ). In contrast to the

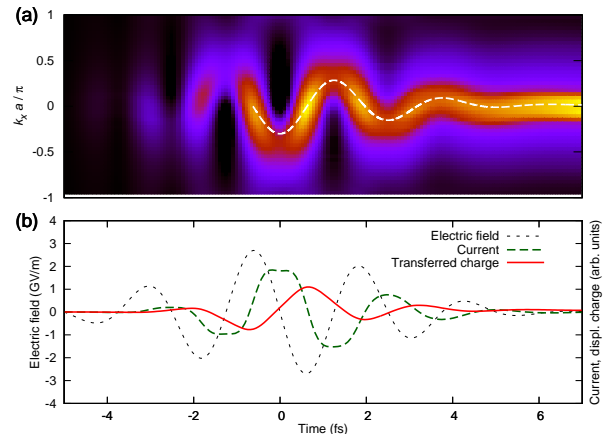


Figure 6. The same as Fig. 5, but for a sine pulse ( $\varphi_{\text{CEP}} = \pi/2$ ). The semiclassical trajectory begins at the first main peak of the laser field, i.e. at  $t = -\pi(2\omega_0)^{-1} \approx -0.6 \text{ fs}$ , and it trespasses  $\mathbf{k} = 0$  at the peak of the next half-cycle, which is the starting point of the second dominant electron trajectory.

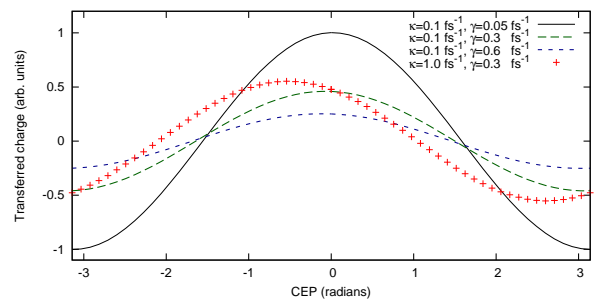


Figure 7. The dependence of the total charge transferred by a laser pulse on its carrier-envelope phase (CEP). The parameters are  $\mathcal{E}_0 = 2 \text{ GV m}^{-1}$ ,  $\tau = 2.3 \text{ fs}$ ,  $\gamma = 0.3 \text{ fs}^{-1}$ . The curve corresponding to  $\kappa = 0.1 \text{ fs}^{-1}$ ,  $\gamma = 0.05 \text{ fs}^{-1}$  has been normalized; the other ones have been scaled by the same number, i.e. the amplitudes of the curves relative to each other are kept fixed. Note that we use  $\kappa = 0.1 \text{ fs}^{-1}$ ,  $\gamma = 0.3 \text{ fs}^{-1}$  in the following.

case of a low field (Fig. 5), the final transferred charge is now negative, which can be interpreted in terms of the semiclassical electron displacement. The dominant electron trajectory, shown as a dashed white line, crosses the lower edge of the Brillouin zone, but it does not reach its upper edge. Since  $\mathbf{v}_c(\mathbf{k}) = 0$  at the edges of the Brillouin zone, the electron is displaced maximally during the time when  $k_x > 0$ . Consequently, the final electron displacement is positive, and the transferred charge is negative.

Note that the temporal evolution of the current in Fig. 8 contains frequency components higher than those of the driving field. The same effect in a different parameter regime was reported to contribute to the generation of nonperturbative high-order harmonics in solids<sup>15</sup>.

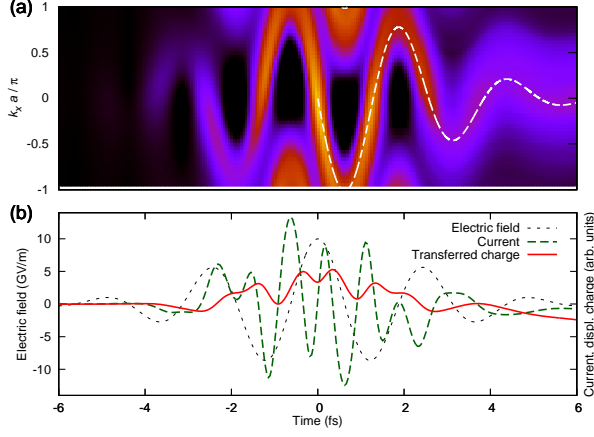


Figure 8. The effect of dynamical Bloch oscillations in a simulation with the following parameters:  $\mathcal{E}_0 = 10 \text{ GV m}^{-1}$ ,  $\varphi_{\text{CEP}} = 0$ ,  $\tau = 2.3 \text{ fs}$ ,  $\kappa = 0.1 \text{ fs}^{-1}$ ,  $\gamma = 0.3 \text{ fs}^{-1}$ . (a) Time evolution of the conduction-band electron population  $n_c(k_x, t)$  for a laser field with an amplitude sufficient for accelerating excited electrons to the edges of the Brillouin zone. The white dashed line represent the solution of Eq. (6) with  $\mathbf{k}(0) = 0$ . (b) The electric field of the laser pulse  $\mathcal{E}_x(t)$ , the induced current density  $j_x$  and the transferred charge  $Q(t)$ .

Figs. 5 and 8 demonstrate that DBOs have a large impact on the CEP dependence of the transferred charge  $Q(\varphi_{\text{CEP}})$ . In Fig. 9, we investigate it more systematically by plotting the normalized transferred charge

$$\tilde{Q}(\varphi_{\text{CEP}}, \mathcal{E}_0) = \frac{Q(\varphi_{\text{CEP}}, \mathcal{E}_0)}{\langle n_c \rangle_{\text{max}}(\mathcal{E}_0)} \quad (13)$$

for different laser intensities. The  $\mathcal{E}_0$ -dependent normalization factor

$$\langle n_c \rangle_{\text{max}}(\mathcal{E}_0) = \Omega^{-1} \max_t \int_{\text{BZ}} n_c(\mathbf{k}, \mathcal{E}_0, t, \varphi_{\text{CEP}} = 0) d^2\mathbf{k}, \quad (14)$$

which is plotted in Fig. 9(c), denotes the maximum of the time dependent average population in the conduction band for  $\varphi_{\text{CEP}} = 0$ .

One immediately observes that the extrema of  $Q(\varphi_{\text{CEP}})$  shift as the laser intensity increases. By inspecting these simulations, we identified DBOs for peak laser fields above  $7 \text{ GV m}^{-1}$ . Below this limit,  $Q(\varphi_{\text{CEP}})$  is approximately proportional to  $\cos(\varphi_{\text{CEP}})$ , and only the amplitude of  $Q(\varphi_{\text{CEP}})$  increases with the peak laser intensity. For intensities high enough to induce DBOs, the extrema of  $Q(\varphi_{\text{CEP}})$  change their positions. For  $\mathcal{E}_0 = 15 \text{ GV m}^{-1}$ , maxima and minima exchange their places.

To relate these observations to the semiclassical analysis, we focus on the cosine pulse and plot the electron displacement at  $t_{\text{max}} = 15 \text{ fs}$  as a function of the peak electric field in Fig. 9(a). We see that this analysis qualitatively explains our numerical results:  $Q(\varphi_{\text{CEP}} = 0, \mathcal{E}_0)$

and  $-s(t_0 = 0, \mathcal{E}_0)$  have their extrema at approximately the same values of the peak electric field  $\mathcal{E}_0$ , the minus sign being due to the negative electron charge.

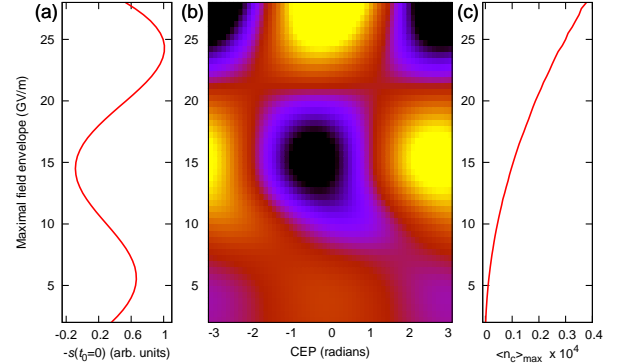


Figure 9. (a) The semiclassical electron displacement (12) times electron charge for  $\varphi_{\text{CEP}} = 0$ ,  $t_0 = 0$  and  $t_{\text{max}} = 15 \text{ fs}$ . The parameters of the laser pulse are  $\tau = 2.3 \text{ fs}$  and  $\omega_0 = 2.51 \text{ fs}^{-1}$ . (b) The normalized transferred charge  $\tilde{Q}$ , defined by Eq. (13), as a function of the CEP and the amplitude of the laser pulse. For dephasing and relaxation, we used  $\kappa = 0.1 \text{ fs}^{-1}$  and  $\gamma = 0.3 \text{ fs}^{-1}$ . (c) The maximal average population in the conduction band  $\langle n_c \rangle_{\text{max}}(\mathcal{E}_0)$ , defined by Eq. (14), for  $\varphi_{\text{CEP}} = 0$ .

Finally, let us return to our model given by Eq. (2) and summarize the physical role of the various processes. Multiphoton excitation and laser-driven motion in the conduction and valence bands are essential for the CEP dependence of the transferred charge, as well as for the appearance of dynamical Bloch oscillations. LO phonon scattering, however, is a process that competes with laser-driven interband motion, and could possibly render the detection of DBOs impossible. According to our calculation, this is not the case even for the large scattering rates known for  $\text{SiO}_2$ <sup>21,22</sup>.

One of our major approximations is using just two bands: a valence and a conduction one. This approximation was made not because we can exclude the involvement of higher conduction or lower valence bands, but because our intention was to clarify the role of Bloch oscillations. In a more realistic description, crossing the edge of a Brillouin zone does not necessarily imply Bragg-like scattering of an electron—transitions to other bands lead to more complicated dynamics<sup>31</sup>, which may, for example, smear the dependencies shown in Fig. 9, especially in the region of the highest intensities. To which extent this happens in a particular measurement will depend on the chosen material, sample preparation, laser wavelength, and other parameters. Even though we neglect these transitions, our results may assist the interpretation of future measurements by recognizing certain features as evidence of Bloch oscillations.

#### IV. SUMMARY

Using a phenomenological model, we have investigated multiphoton injection and laser-driven motion of charge carriers in a wide-gap bulk dielectric exposed to intense few-cycle laser pulses. In comparison with more rigorous quantum models<sup>18,20,32</sup>, where different physical phenomena are relatively difficult to disentangle, our approach lends itself to clarifying the roles played by various processes. Our most important finding is that whenever a laser field drives electrons close to or beyond the edges of the Brillouin zone, Bragg-like reflections of electron waves have a significant impact on CEP-sensitive measurements like those reported in Ref. 18 (the phase shift by  $\pi$  in Fig. 9). At the same time, the role of electron-phonon scattering is limited to reducing the amount of the transferred charge without qualitatively affecting CEP dependencies, even if we assume scattering rates as high as  $\gamma \sim 10^{14} \text{ s}^{-1}$ . The fact that electron-phonon scattering plays a minor role in the high-intensity regime justifies neglecting it in earlier models<sup>18,32</sup>. Our final conclusion is that the detection of the total transferred

charge can be used to measure signatures of dynamical Bloch oscillations in bulk solids. Furthermore, we show that this effect can be qualitatively explained in terms of the semiclassical electron displacement evaluated for dominant electron trajectories.

#### ACKNOWLEDGEMENTS

The authors are indebted to A. Schiffrin, S. Kruchinin, T. Paasch-Colberg, F. Krausz and, particularly, N. Karpowicz for illuminating discussions. This work was supported by the Hungarian Scientific Research Fund (OTKA) under Contract No. T81364 as well as by the projects TÁMOP-4.2.2.A-11/1/KONV-2012-0060 and TÁMOP-4.2.2.C-11/1/KONV-2012-0010 supported by the European Union and co-financed by the European Social Fund. V. S. Y. acknowledges support by the DFG Cluster of Excellence: Munich-Centre for Advanced Photonics.

- 
- \* foldi@physx.u-szeged.hu  
 † vladislav.yakovlev@lmu.de
- <sup>1</sup> F. Bloch, *Zeitschrift für Physik* **52**, 555 (JUL 1929)
  - <sup>2</sup> G. H. Wannier, *Phys. Rev.* **117**, 432 (1960)
  - <sup>3</sup> W. V. Houston, *Phys. Rev.* **57**, 184 (Feb 1940)
  - <sup>4</sup> E. E. Mendez, F. Agulló-Rueda, and J. M. Hong, *Phys. Rev. Lett.* **60**, 2426 (Jun 1988)
  - <sup>5</sup> J. Feldmann, K. Leo, J. Shah, D. A. B. Miller, J. E. Cunningham, T. Meier, G. von Plessen, A. Schulze, P. Thomas, and S. Schmitt-Rink, *Phys. Rev. B* **46**, 7252 (Sep 1992)
  - <sup>6</sup> W. Kuehn, P. Gaal, K. Reimann, M. Woerner, T. Elsaesser, and R. Hey, *Phys. Rev. Lett.* **104**, 146602 (Apr 2010)
  - <sup>7</sup> T. Pertsch, P. Dannberg, W. Elfein, A. Bräuer, and F. Lederer, *Phys. Rev. Lett.* **83**, 4752 (Dec 1999)
  - <sup>8</sup> R. Morandotti, U. Peschel, J. S. Aitchison, H. S. Eisenberg, and Y. Silberberg, *Phys. Rev. Lett.* **83**, 4756 (Dec 1999)
  - <sup>9</sup> R. Sapienza, P. Costantino, D. Wiersma, M. Ghulinyan, C. J. Oton, and L. Pavesi, *Phys. Rev. Lett.* **91**, 263902 (Dec 2003)
  - <sup>10</sup> V. Agarwal, J. A. del Rio, G. Malpuech, M. Zamfirescu, A. Kavokin, D. Coquillat, D. Scalbert, M. Vladimirova, and B. Gil, *Phys. Rev. Lett.* **92**, 097401 (Mar 2004)
  - <sup>11</sup> M. Ben Dahan, E. Peik, J. Reichel, Y. Castin, and C. Salomon, *Phys. Rev. Lett.* **76**, 4508 (Jun 1996)
  - <sup>12</sup> M. Holthaus, *Journal of Optics B: Quantum and Semiclassical Optics* **2**, 589 (2000)
  - <sup>13</sup> J. A. Gruetzmacher and N. F. Scherer, *Review of Scientific Instruments* **73**, 2227 (2002)
  - <sup>14</sup> E. Goulielmakis, M. Schultze, M. Hofstetter, V. S. Yakovlev, and J. Gagnon, *Science* **320**, 1614 (2008), ISSN 0036-8075
  - <sup>15</sup> S. Ghimire, A. D. DiChiara, E. Sistrunk, P. Agostini, L. F. DiMauro, and D. A. Reis, *Nat. Physics* **7**, 138 (2011)
  - <sup>16</sup> S. Ghimire, A. D. DiChiara, E. Sistrunk, U. B. Szafruga, P. Agostini, L. F. DiMauro, and D. A. Reis, *Phys. Rev. Lett.* **107**, 167407 (2011)
  - <sup>17</sup> D. Golde, T. Meier, and S. W. Koch, *Phys. Rev. B* **77**, 075330 (2008)
  - <sup>18</sup> A. Schiffrin, T. Paasch-Colberg, N. Karpowicz, V. Apalkov, D. Gerster, S. Mühlbrandt, M. Korbman, J. Reichert, M. Schultze, S. Holzner, J. V. Barth, R. Kienberger, R. Ernstorfer, V. S. Yakovlev, M. I. Stockman, and F. Krausz, *Nature* **493**, 70 (2013)
  - <sup>19</sup> A. Baltuska, T. Udem, M. Uiberacker, M. Hentschel, and E. Goulielmakis, *Nature* **421**, 611 (2003)
  - <sup>20</sup> V. Apalkov and M. I. Stockman, *Phys. Rev. B* **86**, 165118 (2012)
  - <sup>21</sup> R. C. Hughes, *Phys. Rev. Lett.* **30**, 1333 (Jun 1973)
  - <sup>22</sup> M. V. Fischetti, D. J. DiMaria, S. D. Brorson, T. N. Theis, and J. R. Kirtley, *Phys. Rev. B* **31**, 8124 (Jun 1985)
  - <sup>23</sup> F. Quéré, S. Guizard, P. Martin, G. Petite, H. Merdji, B. Carré, J.-F. Hergott, and L. Le Déroff, *Phys. Rev. B* **61**, 9883 (Apr 2000)
  - <sup>24</sup> C. Kittel, *Introduction to solid state physics*, 8th ed. (Wiley, New York, 2005) pp. 191–194
  - <sup>25</sup> L. W. Casperson, *Phys. Rev. A* **57**, 609 (1998)
  - <sup>26</sup> H. Haug and S. W. Koch, *Quantum Theory of the Optical and Electronic Properties of Semi conductors*, 4th ed. (World Scientific, New Jersey, London, Singapore, 2004)
  - <sup>27</sup> M. Wegener, *Extreme Nonlinear Optics: An Introduction*, Advanced Texts in Physics (Springer, 2004) ISBN 9783540222910
  - <sup>28</sup> T. Otobe, M. Yamagiwa, J.-I. Iwata, K. Yabana, T. Nakatsukasa, and G. F. Bertsch, *Phys. Rev. B* **77**, 165104 (Apr 2008)
  - <sup>29</sup> O. D. Mücke, *Phys. Rev. B* **84**, 081202 (Aug 2011)
  - <sup>30</sup> E. Yablonovitch, J. P. Heritage, D. E. Aspnes, and Y. Yafet, *Phys. Rev. Lett.* **63**, 976 (Aug 1989)



- <sup>31</sup> B. M. Breid, D. Witthaut, and H. J. Korsch, *New Journal of Physics* **8**, 110 (2006)
- <sup>32</sup> S. Y. Kruchinin, M. Korbman, and V. S. Yakovlev, *Phys. Rev. B* **87**, 115201 (Mar 2013)